

Magnetic field imaging with atomic Rb vapor

Eugeniy E. Mikhailov and I. Novikova

Department of Physics, The College of William & Mary, Williamsburg, VA 23187

M. D. Havey

Department of Physics, Old Dominion University, Norfolk, VA 23529

F. A. Narducci

EO Sensors Division, Naval Air Systems Command, Patuxent River, MD 20670

(Dated: June 19, 2018)

We demonstrate the possibility of dynamic imaging of magnetic fields using electromagnetically induced transparency in an atomic gas. As an experimental demonstration we employ an atomic Rb gas confined in a glass cell to image the transverse magnetic field created by a long straight wire. In this arrangement, which clearly reveals the essential effect, the field of view is about $2 \times 2 \text{ mm}^2$ and the field detection uncertainty is 0.14 mG per $10 \text{ }\mu\text{m} \times 10 \text{ }\mu\text{m}$ image pixel.

Efforts to develop measurement techniques for precision magnetometry have a long and successful history in atomic physics [1, 2, 3, 4, 5]. Some recent advances in development of compact atomic magnetometers take advantage of the unique properties of the electromagnetically induced transparency (EIT) effect and the existence of coherently produced optical dark states, which can be extremely sensitive to external fields [6]. Here, we propose the idea of a three axis magnetometer for dynamic imaging of magnetic field gradients based on EIT using state of the art imaging technologies. We also demonstrate the essential idea with a one axis (two dimensional) prototype. As described later, a fully implemented three dimensional magnetic gradiometer promises both high precision and useful visualization tools for both static and dynamic magnetically complex environments. The potential applications of this technique range from essentially fundamental (e.g. precision searches for magnetic monopoles [7]) to quite applied, such as, for example, precise monitoring of the magnetic environment in medical applications or quantum information experiments [8, 9].

The proposed approach relies on the spectrally ultra-narrow transmission resonances observed under EIT conditions in an atomic gas. These resonances are associated with the coherent non-interacting (dark) states in a three-level Λ system formed under the combined action of two electromagnetic fields in two-photon Raman resonance with two long-lived metastable states of an atom. The width of the EIT resonances is determined by the intensities of the laser field and the lifetime of the ground-state coherence, and can be as small as a few Hz [10, 11]. Such spectral sensitivity makes this effect very promising for precision metrology. In particular, the spectral location of the transparency resonance depends on the external magnetic field when the Λ -system is based on the magnetic field-sensitive Zeeman sublevels. Moreover, if the magnetic field is spatially varying transversely in a plane orthogonal to the probe beam's \mathbf{k} vector, the resonances will occur at different spatial locations for dif-

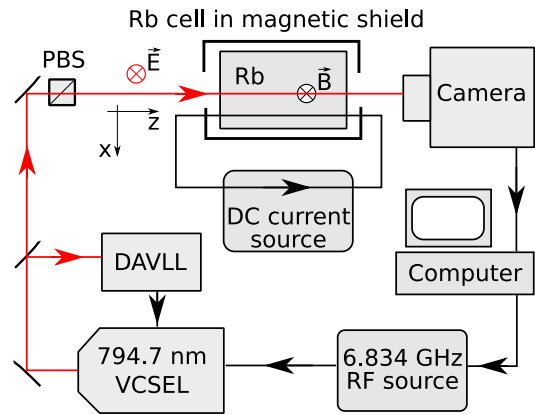


FIG. 1: A schematic diagram of the experimental configuration.

ferent two-photon resonance detunings. Thus, the spatial distribution of transmitted intensity will display a transverse image of the spatial regions where the two photon resonance condition is satisfied. Recording a series of such images for various two-photon frequencies can create a spatial map of the transverse magnetic field. Combining such measurements made in three orthogonal directions (formed from, for example, three independent arrangements) allows six elements of the $\nabla\mathbf{B}$ tensor to be measured. According to the source free Maxwell's Equations, there are four constraints on the nine components of $\nabla\mathbf{B}$, implying a desirable unit redundancy in each set of six measurements.

In this Letter we illustrate the concept by imaging the magnetic field produced by a long straight wire carrying a steady current I running along the length of a Rb vapor cell. Since in our experiment we are able to detect the light transmission through the cell only in one direction, we took extreme care to make the wire as coaxial as possible with the laser beam to remove any variation of the magnetic field along the optical axis. The aim is then to measure the resulting transverse variation of the magnetic field across the laser beam by imaging the

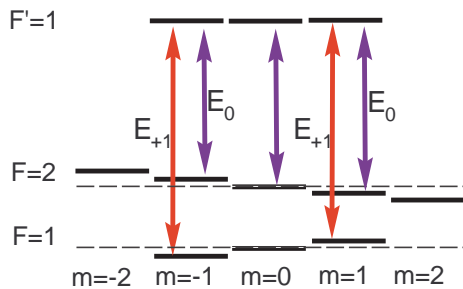


FIG. 2: Energy level diagram illustrating the Zeeman transitions essential to the EIT Λ schemes formed by the carrier E_0 and the first modulation sideband E_{+1} .

transverse variations of the transmitted light intensity as a function of the two-photon detuning.

A schematic of the experimental setup is shown in Fig. 1. We use a vertical-cavity surface emitting laser (VCSEL) directly phase-modulated at 6.834 GHz (a ^{87}Rb hyperfine frequency), and use the fundamental (carrier) laser frequency and one of the side bands to produce the two optical fields required for EIT observation. The laser beam with total power 200 μW and a slightly elliptical Gaussian profile [waist sizes 1.8 mm and 1.4 mm full width half maximum (FWHM)], was directed into the cylindrical Pyrex cell (with length 75 mm and diameter 22 mm) containing isotopically enriched ^{87}Rb vapor and 15 Torr of Ne buffer gas. The cell was mounted inside a three-layer magnetic shielding to reduce stray laboratory magnetic fields with the suppression factor of at least 1000, and its temperature was actively stabilized at 322 K by regulating the current through a bifilar heater wire wrapped around the innermost shield.

The magnetic field producing wire was mounted parallel to the laser beam at a distance $\rho_0 = 20.1 \pm 0.2$ mm, and connected to a low-noise current supply operating at $I = 438 \pm 1$ mA. Then the magnetic field outside the wire produced by this current is orthogonal to the light propagation direction, and can be estimated as (neglecting the effects of the magnetic shielding):

$$B(\rho) = \frac{\mu_0 I}{2\pi\rho} \quad (1)$$

where ρ is the distance from the center of the wire, and μ_0 is permeability of free space. If we let the laser beam's wave vector and the direction of current flow define the z -direction, the curves of constant magnetic field B are then circles in the x - y plane and centered on the wire. For a given two-photon detuning the EIT resonance conditions are obeyed only for a given value of the magnetic field, and thus for a large laser beam we in general expect to observe a corresponding "bright" circular arc in the transmission spatial profile, with the radius of the arc depending on the set two-photon detuning. In our experimental arrangements, however, the laser beam diameter is small compare to the distance to the wire ρ_0 , so the

magnetic field across the laser beam is mainly along the y -axis and changes linearly with small displacement δx :

$$B(\rho) = \frac{\mu_0 I}{2\pi\rho_0} \left(1 - \frac{\delta x}{\rho_0}\right) \quad (2)$$

For the measurements, the laser frequency was tuned such that the stronger optical field (unmodulated carrier) was resonant with the $5 S_{1/2} F = 2 \rightarrow 5 P_{1/2} F' = 1$ transition of ^{87}Rb , while the frequency of the +1 modulation sideband matched the $5 S_{1/2} F = 1 \rightarrow 5 P_{1/2} F' = 1$ transition. The laser output was linearly polarized. In this configuration there are two possible Λ -systems for $F = 1, 2; m_F = \pm 1 \rightarrow F' = 1; m_{F'} = \pm 1$ that produce EIT resonances at two-photon detunings $\Delta\nu = \Delta_{HFS} \pm 2g_m B$ (shown in Fig. 2), where $g_m = 0.7$ MHz/G is the gyromagnetic ratio for ^{87}Rb [13]. We also adjusted the power of the VCSEL modulation signal to cancel the light shift of the EIT resonances, and to avoid the effects of non-uniform spatial distribution of the laser beam on the measured resonance position [14]. For our experimental conditions such cancellation occurred for a sideband/carrier intensity ratio of 0.75. Also, we analyzed only the area of the image where the intensity of the beam exceeds half of its maximum value.

To map the spatial variation of the magnetic field, we stepped the VCSEL modulations frequency in a 20 kHz range around one of the EIT resonances in 200 Hz increments, taking images of the transmitted laser beam profile using a digital camera (Unibrain Fire-i 511b). The dominant source of noise in our experiment was due to the phase-to-amplitude noise conversion of the VCSEL large phase noise (the linewidth of the laser was ≈ 100 MHz) by the absorption in the cell. To reduce the detection noise of the image, we recorded and averaged 200 sequential images grabbed from the camera, which operated at a 30 frame per second rate for any particular two photon detuning. Even then the detection noise is larger than the digital resolution of the 12 bit analog-to-digital converter of the camera. For each pixel of the image we plotted the intensity as a function of the two-photon detuning, as shown in Fig. 3(a). Then we located the position of the EIT maximum (and correspondingly the value of the local magnetic field). After analyzing the transmission for every pixel we obtained a spatial map of magnetic field, shown in Fig. 3(b). The average variance between two sequential runs allowed us to put an upper limit on the experimental uncertainty of the magnetic field measurements $\Delta B = 0.14$ mG for every 10 μm pixel.

We compare the measured magnetic field with numerical calculation of the magnetic field generated by a long straight wire inside a cylindrical magnetic shield. Since the inner shield modifies the magnetic field from the simple Biot-Savart law given by Eq. 1, we used a finite element (FEM) analysis program to calculate the expected magnetic field distribution inside the laser beam [15], as shown in Fig. 3(c). The rather large uncertainty of our FEM model is governed by possible variations in each

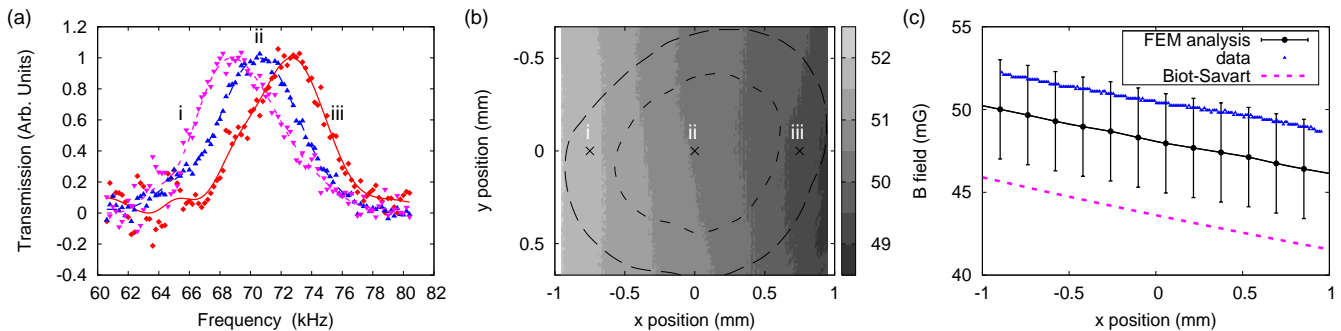


FIG. 3: (a) Transmission through the cell detected at three different camera pixels [marked in (b)] as functions of the two-photon detuning. Solid lines show low-pass filtered data used to determine the maximum transmission position. (b) Map of the magnetic field strength. Dashed lines mark the 75% and 50% levels of the maximum laser beam intensity. (c) Experimentally measured magnetic field slice of the map (b) along $y = 0$ as a function of x position, and the theoretically calculated magnetic fields using the Biot-Savart law [Eq.(1)] and a finite element analysis. The error bars in the FEM curve represent the variation in the calculated magnetic field due to ± 1 mm uncertainty in the magnetic shielding position with respect to the wire and the laser beam.

shield's diameter, thickness, and imperfect cylindrical shapes, as well as the uncertainty in the location of the wire inside of the shielding. For instance, Fig. 3(c) illustrates that displacement of the shielding position as small as 1 mm is sufficient to match the FEM simulations with the experimental measurements.

The demonstrated sensitivity of our apparatus ($\approx 14\mu\text{G}/\mu\text{m}$) is limited by the transmitted intensity fluctuations of the broadband VCSEL output. We expect much better sensitivity for narrow-band electromagnetic fields, which should dramatically reduce the amount of amplitude noise in the output. A good candidate for such a source, for example, could be a narrow band external cavity diode laser followed by an external phase modulator.

We can estimate the precision of the magnetic field measurements ΔB due to the uncertainty in two-photon detuning frequency corresponding to the maximum transmission for a given signal-to noise ratio S/N [16]:

$$\Delta B \simeq \frac{1}{2g_m} \frac{\gamma}{S/N\sqrt{n}}. \quad (3)$$

In this expression we assume that the EIT resonance has Lorentzian shape with a known FWHM γ , and n is the number of sampling points per resonance width. The optimal frequency span in this case should exceed, or be comparable with, the value γ , with $n > 5 - 10$ for each recorded trace to avoid numerical errors in fitting related to discretization artifacts.

We note that the ultimate relative sensitivity of our method should be similar to that of atomic clocks, based on the same operational principle [12]. In particular, miniature atomic clocks demonstrate a fractional stabil-

ity on the order of $10^{-11} - 10^{-12}/\sqrt{\text{Hz}}$. However, in practice the performance of the magnetic field imager may be limited by other factors, such as digital noise or the limited optical sensitivity per pixel of a charge coupled camera. These, and other factors including the essential role of longitudinally varying magnetic fields, are currently under investigation.

In conclusion, we propose a new method of dynamic imaging of a magnetic field by detecting spatial and temporal variations in transmission of light through an atomic sample under conditions of electromagnetically induced transparency. In general, this method can be applied to measurements of three-dimensional magnetic field maps. To demonstrate the basic operational principle, we reconstructed the spatial distribution of the transverse magnetic field created by a current-carrying long straight wire, running along an atomic Rb vapor cell, with the precision of $14\mu\text{G}/\mu\text{m}$ inside the $1.8 \times 1.4 \text{ mm}^2$ laser beam cross-section. Our prototype apparatus can be readily scaled up for either a larger or smaller detection area by adding a zooming telescope in front of the camera (although the total power of the laser would have to be reoptimized). Also, since our prototype experiment was performed using a VCSEL, we expect that this method can be used with recently developed chip-scale systems for miniature atomic clocks and magnetometers [17].

The authors thank D. Malyarenko and J. P. Davis for useful discussions, and S. Aubin for his help with the image acquisition code. This research was supported by NSF grants PHY-0758010, PHY-0654226, Jeffress Research grant J-847, ONR grants N0001409WX20679 and In-House Laboratory Innovative Research (ILIR).

[1] D. Budker and M. V. Romalis, Optical magnetometry, Nature Phys. **3**, 227 (2007).

[2] C. Affolderbach, M. Stähler, S. Knappe and R. Wynands,

- An all-optical high-sensitivity magnetic gradiometer, *Appl. Phys. B* **75**, 605 (2002).
- [3] I. K. Komins, T. W. Kornack, J. C. Allred, and M. V. Romalis, A subfemtotesla multichannel atomic magnetometry, *Nature* **422**, 596 (2003).
- [4] S. Xu, S. M. Rochester, V. V. Yashchuk, M. H. Donaldson, and D. Budker, Construction and applications of an atomic magnetic gradiometer based on nonlinear magneto-optical rotation, *Rev. Sci. Instr.* **77**, 083106 (2006).
- [5] M. Vengalattore, J. M. Higbie, S. R. Leslie, J. Guzman, L. E. Sadler, and D. M. Stamper-Kern, High-resolution magnetometry with spinor bose-einstein condensate, *Phys. Rev. Lett.* **98**, 200801 (2007).
- [6] M. Fleischhauer, A. Imamoglu, and J. P. Marangos, Electromagnetically induced transparency: Optics in coherent media, *Rev. Mod. Phys.* **77**, 633 (2005).
- [7] P. A. M. Dirac, Quantised singularities in the electromagnetic field, *Proc. Royal Soc. London* **133**, 60 (1931).
- [8] M. D. Lukin, Colloquium: Trapping and manipulating photon states in atomic ensembles, *Rev. Mod. Phys.* **75**, 457 (2003).
- [9] H. J. Kimble, The quantum internet, *Nature* **453**, 1023 (2008).
- [10] D. Budker, V. Yashchuk, and M. Zolotarev, Nonlinear Magneto-optic Effects with Ultranarrow Widths, *Phys. Rev. Lett.* **81**, 5788 (1998).
- [11] M. Erhard and H. Helm, Buffer-gas effects on dark resonances: theory and experiment, *Phys. Rev. A* **63**, 043813 (2001).
- [12] J. Vanier, Atomic Clocks Based on Coherent Population Trapping: a Review, *Appl. Phys. B* **81**, 421 (2005).
- [13] For arbitrary orientation of the laser polarization with respect of the magnetic field vector various Λ system will be formed by both π and σ_{\pm} transitions, resulting in EIT resonances at $0, \pm g_m B$ and $\pm 2g_m B$ two-photon detunings. Careful analysis of relative amplitudes of these resonances may allow measurements of not only the magnitude but also the direction of the magnetic field.
- [14] S. A. Zibrov, I. Novikova, D. F. Phillips, R. L. Walsworth, A. S. Zibrov, V. L. Velichansky, A. V. Taichenachev, and V. I. Yudin, Coherent population trapping resonances with linearly polarized light for all-optical miniature atomic clocks, to be submitted (2009).
- [15] We used FEMM available at <http://femm.foster-miller.net/wiki/HomePage> (accessed July 2009).
- [16] A. G. Marshall and F. R. Verdun, *Fourier Transforms in NMR, Optical, and Mass Spectrometry*, (Elsevier, Amsterdam, 1990).
- [17] V. Shah, S. Knappe, P. D. D. Schwindt, and J. Kitching, Subpicotesla atomic magnetometry with a microfabricated vapour cell, *Nature Photonics* **1**, 649 (2007).